Journal of Membrane Science 548 (2018) 157–164

Contents lists available at ScienceDirect

Journal of Membrane Science

journal homepage: www.elsevier.com/locate/memsci

Micropore structure stabilization in organosilica membranes by gaseous catalyst post-treatment

A. Petra Dral[a], Ernst R.H. van Eck[b], Louis Winnubst[c], Johan E. ten Elshof[a,*]

[a] Inorganic Materials Science, MESA+ Institute for Nanotechnology, University of Twente, P.O. Box 217, 7500 AE Enschede, The Netherlands
[b] Solid State NMR, Institute for Molecules and Materials, Radboud University, P.O. Box 9010, 6500 GL Nijmegen, The Netherlands
[c] Inorganic Membranes, MESA+ Institute for Nanotechnology, University of Twente, P.O. Box 217, 7500 AE Enschede, The Netherlands

ARTICLE INFO

Keywords:
Micropore stabilization
Organosilica
Catalyst post-treatment
Hydrolysis
Molecular sieving membrane

ABSTRACT

A post-treatment involving repeated exposure to gaseous HCl alternated with heating is demonstrated to strongly accelerate the recently reported structural evolution in organically bridged silica networks. Films, powders and membranes derived from 1,2-bis(triethoxysilyl)ethane were exposed to in-situ synthesized HCl gas, alternated with heat treatments at 150–300 °C in air or N_2. The film thickness, network condensation, chemical integrity and micropore structure were monitored with X-ray reflectivity, ^{29}Si direct-excitation magic-angle spinning nuclear magnetic resonance, Fourier-transform infrared spectroscopy and gas permeation. Treatment with HCl was found to predominantly catalyze hydrolysis, enabling network optimization via iterative bond breakage and reformation. Network shrinkage, widening or opening of the smallest pores and densification of the overall pore structure were accelerated while the ethylene bridges remained intact. The achieved acceleration of material evolution makes iterative hydrolysis and condensation a promising approach for increasing the long-term micropore stability of molecular sieving membranes.

1. Introduction

Hybrid organosilica networks, in which part of the Si-O-Si linkages are replaced by Si-R-Si, provide a valuable combination of inorganic and organic material properties. For membrane applications, the introduction of organic bridging segments to microporous silica yields networks with tunable pore sizes and affinities and a highly superior hydrothermal stability [1–8]. Hybrid organosilica membranes have replaced inorganic silica membranes in various molecular sieving applications under hydrothermal conditions. However, this new generation of membranes displays a slow ongoing flux decline during operation at 95–150 °C for more than a year [1,2,9], causing practical difficulties in industrial processes. To date, this problem has not been solved.

Recently, we reported a detailed study on long-term consolidation in powders, films and membranes derived from 1,2-bis(triethoxysilyl) ethane (BTESE) [10]. Subtle but persistent chemical and structural changes were demonstrated to continue for days to weeks at temperatures up to 300 °C without approaching an end state. Ongoing chemical condensation was accompanied by network shrinkage and decreasing density. This led to a decreasing gas permeance through relatively large pores > 0.4 nm but an increasing gas permeance through small pores ~0.3 nm. The structural changes were speeded up by exposure to HCl vapor, which was previously reported as a method to increase condensation and reduce micropore sizes in BTESE-derived membranes by Wang et al. [11,12]. The process observed in our recent study was proposed to be the origin of the problem of slow flux decline in industrially employed organically bridged silica membranes over periods of months to years. As for solutions to this instability issue, we proposed a post-synthesis treatment to catalyze both condensation and hydrolysis in a combined or alternating fashion. This facilitates evolution of the network into a more favorable configuration via iterative reconnections. This iterative approach differs from the single-step catalyst post-treatments generally reported in literature for (organo)silica materials. Liquid-phase hydrothermal treatment with NH_4OH and HCl has been reported to increase the structural stability and condensation degree and tune textural properties of mesoporous inorganic silica [13–15]. Vapor-phase HCl treatment has been used to tune the micropore size and increase the condensation degree of microporous ethylene-bridged membranes [11,12,16].

The present study introduces a post-treatment involving iterative hydrolysis and condensation to achieve extensive reorganization and stabilization of organosilica networks in a controlled fashion. The chemical reaction scheme shown in Fig. 1a. BTESE-derived films,

* Corresponding author.
E-mail addresses: a.p.dral@utwente.nl (A.P. Dral), e.vaneck@nmr.ru.nl (E.R.H. van Eck), a.j.a.winnubst@utwente.nl (L. Winnubst), j.e.tenelshof@utwente.nl (J.E. ten Elshof).

https://doi.org/10.1016/j.memsci.2017.11.014
Received 11 September 2017; Received in revised form 1 November 2017; Accepted 4 November 2017
Available online 06 November 2017
0376-7388/ © 2017 Elsevier B.V. All rights reserved.

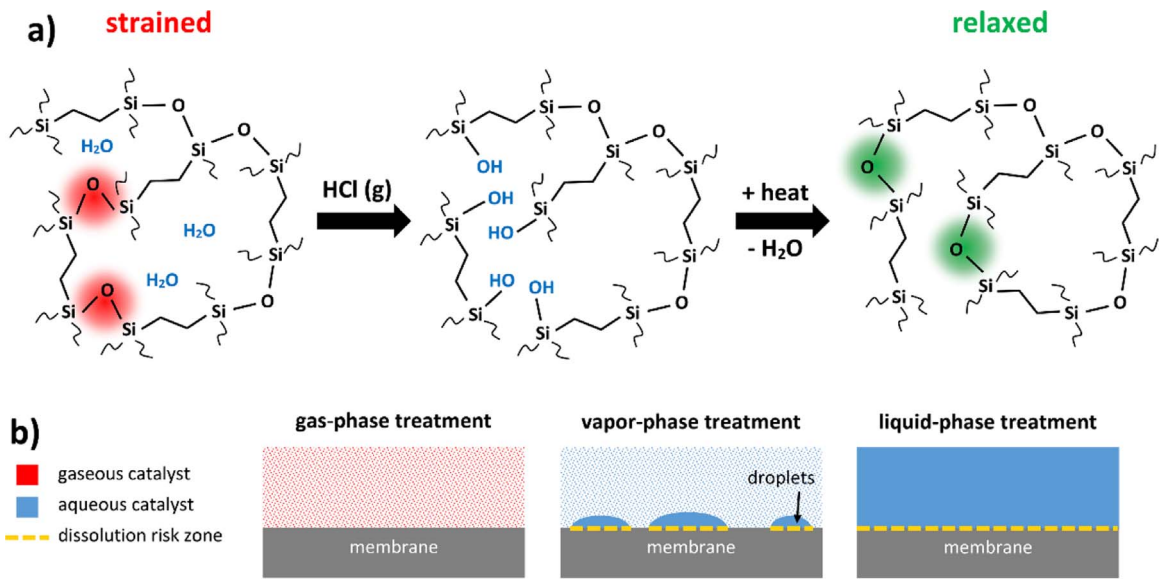

Fig. 1. a) Chemical reaction scheme of network stabilization. b) Schematic representation of gas-phase, vapor-phase and liquid-phase catalyst treatments.

powders and membranes were repeatedly exposed to in-situ synthesized HCl gas alternated with heat treatments. Several process parameters were varied to study the mechanism of network evolution and to commence process optimization. The film thickness, network condensation, chemical integrity and micropore structure were monitored with X-ray reflectivity (XRR), ^{29}Si direct-excitation magic-angle spinning nuclear magnetic resonance (^{29}Si DE-MAS-NMR), Fourier-transform infrared spectroscopy (FTIR) and gas permeation (GP). Though some water is required for the reactions, this gas-phase catalyst treatment involves much lower quantities of water (i.e. only atmospheric and adsorbed moisture) than previously reported liquid-phase and vapor-phase catalyst treatments. This eliminates the risk of material dissolution and pinhole formation in either the organosilica top layer or its support when applied to molecular sieving membranes, as schematically depicted in Fig. 1b.

2. Experimental

2.1. Chemicals

1,2-bis(triethoxysilyl)ethane (97% purity) was obtained from ABCR. Nitric acid (70 wt% aqueous solution), 1-butanol (99.8% purity) and Mowiol 8–88 polyvinyl alcohol were obtained from Sigma Aldrich. Ethanol (dehydrated, 99.99% purity) was obtained from VWR. Sulfuric acid (≥95% purity) was obtained from Fluka. Sodium chloride (99.7% purity) was obtained from J.T. Baker.

2.2. Powder and film preparation

BTESE-derived sols and powders were prepared as reported elsewhere [10]. 3.24 mL demi water and 0.798 mL aqueous HNO_3 (65 wt %) were added to 50 mL dry ethanol at room temperature, followed by adding 11.12 mL BTESE under stirring. The mixture was then heated to 60 °C in an oil bath for 3 h and cooled to room temperature in a water bath. Powder was obtained by drying the sol overnight in plastic petri dishes and grinding the resulting glass by ball milling. Powders of multiple synthesis batches were mixed to obtain one homogeneous stock for all experiments reported here. BTESE-derived films (50–55 nm) were prepared by mixing part of the sol for powder with 1-butanol in a 2:3 volume ratio and spin coating on silicon wafer substrates. The silicon substrates were cleaned with ethanol prior to coating. Each substrate was coated with 20 μL solution at a spinning rate of 10.000 rpm for 10 s. The films were dried on a hot plate in air at 200 °C for 30 min. All samples were stored under ambient conditions.

2.3. Membrane preparation

Membranes with BTESE-derived top layers having effective pore sizes of either > 0.4 nm or ~0.3 nm were prepared as reported elsewhere [10]. Polished AKP30 α-alumina disks were obtained from Cobra Technologies BV and used as membrane supports. The supports were coated with a mesoporous γ-alumina layer and a BTESE-derived top layer, both applied under cleanroom 1000 conditions with a Velterop DA 3960/02 dip coater with a dipping speed of 1.4 cm s^{-1}. The preparation of the mesoporous γ-alumina coating was derived from the method described by Uhlhorn et al. [17]. 2.25 g PVA was added to 75 g 0.05 M aqueous HNO_3 solution and the mixture was heated under stirring to 80 °C for 2 h. 20 mL of the resulting PVA solution was filtered with a 0.8 μm filter and added to 30 mL 0.8 μm filtered boehmite sol prepared according to Uhlhorn et al. [17], followed by stirring and coating. The mesoporous γ-alumina layers were calcined at 650 °C in air for 3 h with heating and cooling rates of 1 °C min^{-1}. BTESE-derived top layers with > 0.4 nm pores were made with the sol recipe for powders. BTESE-derived top layers with ~0.3 nm pores were made as reported by Castricum et al. [6] with a sol of 35 mL dry ethanol, 2.91 mL demi water, 0.614 mL aqueous HNO_3 (65 wt%) and 11.0 mL BTESE prepared under otherwise identical conditions. Both sols were diluted with dry ethanol in a 1:1 volume ratio and filtered with a 0.2 μm filter before coating. The BTESE-derived top layers were cured at 300 °C in N_2 for 24 h with heating and cooling rates of 5 °C min^{-1}. All membranes were stored under ambient conditions.

2.4. X-ray reflectivity

Thickness measurements of films at 300 °C were done with X-ray reflectivity (XRR) on a PANalytical X'Pert PRO system equipped with an Empyrean tube with Cu anode, a parabolic W/Si mirror, an Anton Paar Domed Hot Stage 900 and a proportional Xe point detector. The films were kept under N_2 flow and were heated to 300 °C for varying periods of time with heating and cooling rates of 60 °C min^{-1}. Reflectivity curves were measured in-situ every 10 min. Thickness measurements of films at room temperature were done on a PANalytical X'Pert PRO system equipped with an Empyrean tube with Cu anode, a parallel beam mirror and a PIXcel^{1D} detector. Thickness values were obtained

by fitting the reflectivity oscillations between θ = 0.5–1° in X'Pert Reflectivity software.

2.5. ^{29}Si nuclear magnetic resonance spectroscopy

^{29}Si nuclear magnetic resonance spectra were obtained ex-situ at a field of 7.05 T with direct excitation and magic angle spinning using a Chemagnetics 9.5 mm pencil probe, resonant for ^{1}H at 300.15 MHz and ^{29}Si at 59.595 MHz. Spectra were acquired with a 3.8 µs pulse, 25 kHz proton decoupling (Spinal), 4 kHz spinning rate, 320 scans per sample and a recycle delay of 500 s, ensuring that the acquired data was quantitative (^{29}Si relaxation time $T_1 \times 5 < 500$ s, determined via a Torchia experiment with cross-polarization). TheT^1, T^2 and T^3 ratios and the Q^2, $Q^3$and Q^4 ratios were determined by spectrum deconvolution. First the cross-polarization spectra were fitted with three Gaussian components, because the signal-to-noise ratio of these spectra was significantly higher than that of the direct-excitation spectra. Peak parameters thus determined were used to deconvolute the direct-excitation spectra, fixing the width and position of the components but not the amplitude. The ratio of T to Q species was determined by integrating the direct-excitation spectra over the relevant regions (spinning side bands were added to the T peaks).

2.6. Gas permeation

Single-gas permeation measurements were performed with a Poseidon Convergence Inspector. The top layer of the membrane was positioned at the feed side. After heating to 200 °C under N_2 flow the permeance was measured for H_2 during 10 h. H_2 was chosen because of its small size; no reactions with the membrane were expected. Then the permeance was measured for He, He, H_2, He, N_2, He, CH_4, He and CO_2 (measured in this order), all during 40 min. He segments were inserted to remove residues of the preceding gas. Some membranes were then subjected to a HCl treatment and/or heating to 300 °C outside the permeation set-up and placed back in the set-up to measure H_2 during 19 h and the series of gases for 40 min each, both repeated three times (78 h permeation in total). The membranes were then again heated to 300 °C outside the permeation set-up and placed back again to measure H_2 during 19 h and the series of gases for 40 min each, both repeated three times (78 h permeation in total). The pressure difference for all measurements was 2 bar and the system was flushed for approximately 5 min after changing gases. The membranes were kept at 200 °C during all measurements.

2.7. HCl treatment

All samples were consolidated at 300 °C in N_2 for at least 3 h prior to HCl treatment. Samples were exposed to HCl gas in a closed square 500 mL glass bottle equipped with two glass petri dishes as schematically shown in Fig. 2. For the sake of safety, the experiments were done

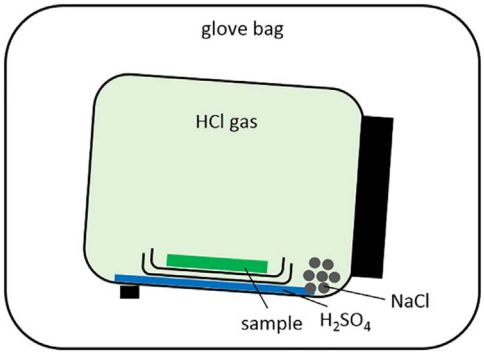

Fig. 2. Schematic representation of the experimental set-up for HCl treatments.

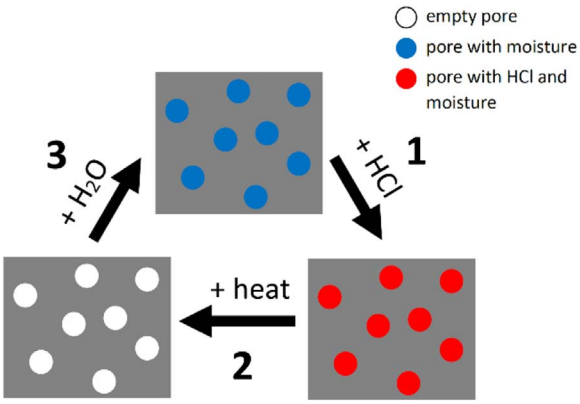

Fig. 3. Schematic representation of a HCl treatment cycle. The sample in hydrated state was exposed to gaseous HCl (1), heated (2) and rehydrated (3).

inside a glove bag in a fume hood. The sample was placed in the inner petri dish and 2.88 mL H_2SO_4 was added on the bottom of the bottle outside the petri dishes. A stoichiometric amount of NaCl (3.15 g) was added to the H_2SO_4 and the glass bottle was closed. The bottle was swirled gently and was then placed in a slightly tilted fashion to enhance mixing of H_2SO_4 and NaCl. After exposure of the sample to the generated HCl gas, the petri dish with the sample was taken out of the bottle and out of the glove bag. The sample was heated instantly to 150 °C in air, 200 °C in air or 300 °C in N_2 and was then rehydrated at room temperature in the ambient (powders and films) or in a humidified atmosphere (membranes). The periods of time for HCl exposure, waiting before heating, heating and rehydration were varied. The procedure was repeated up to 15 times. The details of each individual sample are given in the text and Figure captions of the corresponding results.

3. Results and discussion

All BTESE-derived materials were consolidated at 300 °C in N_2 for at least 3 h and were then repeatedly exposed to HCl. A complete HCl treatment cycle involved three stages, as schematically shown in Fig. 3. First, the sample in its usual hydrated state was exposed to gaseous HCl at room temperature. HCl was formed in-situ from NaCl and liquid H_2SO_4. Second, the sample was heated to promote dehydration and dehydroxylation. Third, the sample was placed in the ambient or a humidified atmosphere to allow rehydration and rehydroxylation.

3.1. Film thickness and hydroxyl concentration

The effect of HCl treatments on the structural evolution in BTESE-derived films was investigated by monitoring the film thickness. Fig. 4a shows the shrinkage behavior in time at 300 °C as measured in-situ with XRR. After 3 h at 300 °C the films were taken out for HCl treatment and were then heated to 300 °C again for 14 h. Exposure to HCl gas for one period of 24 h led to about 1% additional shrinkage and repeated exposure for four times 1 h with intermediate heating to 200 °C for 10 min increased the shrinkage with 6%. Reference experiments with only liquid H_2SO_4 (not in direct contact with the sample) indicated no effect of H_2SO_4 fumes.

^{29}Si DE-MAS-NMR measurements were done to investigate the chemistry underlying the HCl effect. HCl can catalyze both hydrolysis and condensation reactions and either of them can induce film shrinkage. Hydrolysis can facilitate network compaction by reducing its connectivity and thus increasing its mobility, enabling a transition towards a more optimal packing. Condensation can drive network compaction by increasing the connectivity and thus pulling network segments close to each other. Fig. 4b shows the hydroxyl concentration in BTESE-derived powders after repeated cycles of exposure to HCl gas for

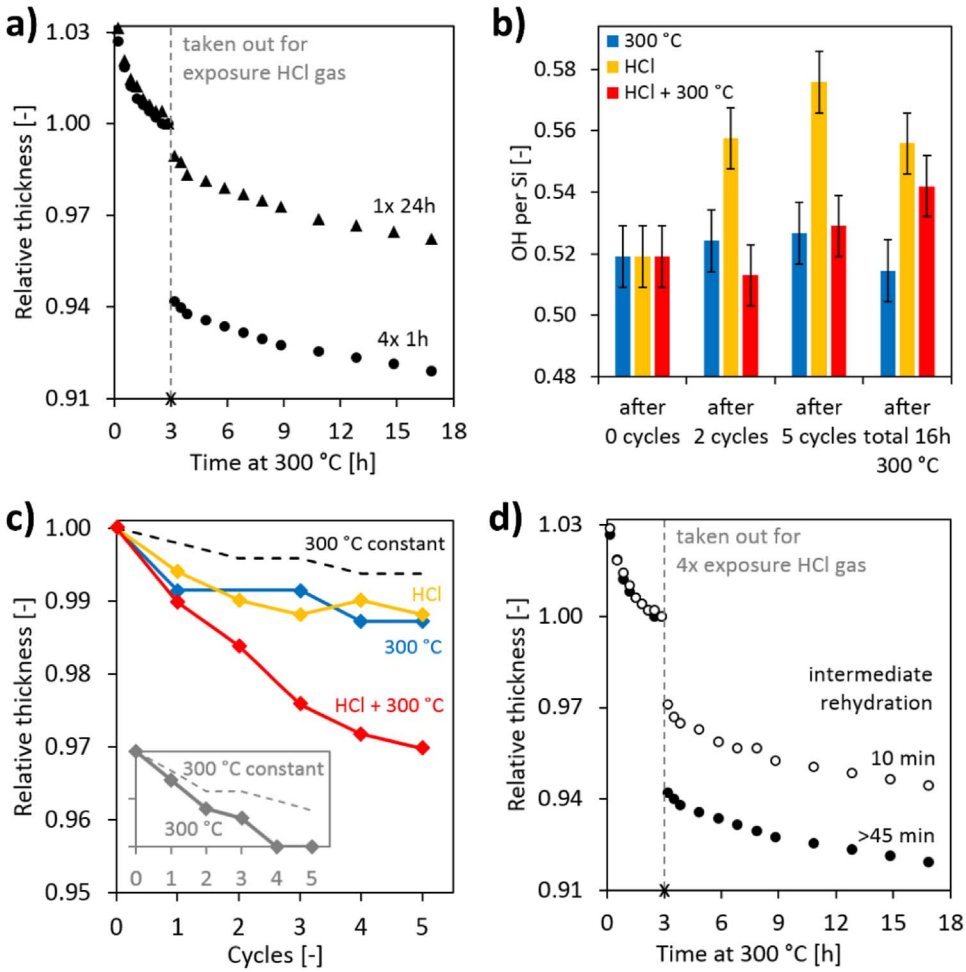

Fig. 4. Thickness of BTESE-derived films as measured with XRR and hydroxyl concentration of BTESE-derived powders as measured with ^{29}Si DE-MAS-NMR. a) Thickness monitored at 300 °C in N_2 before ($t < 3$ h) and after ($t > 3$ h) exposure to HCl gas at room temperature for either one period of 24 h (triangles) or four cycles of 1 h exposure to HCl gas, 20 min waiting, 10 min heating to 200 °C in air and > 45 min rehydration in the ambient (circles). b) Hydroxyl concentration measured at room temperature during five cycles of 10 min heating to 300 °C in N_2 and > 3 h rehydration in the ambient (blue), five cycles of 10 min exposure to HCl gas and > 3 h waiting in the ambient (yellow) or five cycles of 10 min exposure to HCl gas, 10 min waiting, 10 min heating to 300 °C in N_2 and > 3 h rehydration in the ambient (red). A final heating step was done to bring all samples on a total of 16 h at 300 °C. c) Thickness monitored at room temperature during five cycles of 10 min heating to 300 °C in N_2 and > 3 h rehydration in the ambient (blue), five cycles of 10 min exposure to HCl gas and > 3 h waiting in the ambient (yellow) or five cycles of 10 min exposure to HCl gas, 10 min waiting, 10 min heating to 300 °C in N_2 and > 3 h rehydration in the ambient (red). The dotted line represents film shrinkage under constant heating at 300 °C. The inset shows shrinkage after cycles of heating to 300 °C for 30 min d) Thickness monitored at 300 °C before ($t < 3$ h) and after ($t > 3$ h) four cycles of 1 h exposure to HCl gas, 20 min waiting, 10 min heating to 200 °C in air and 10 min or > 45 min rehydration in the ambient. (For interpretation of the references to color in this figure legend, the reader is referred to the web version of this article.)

10 min with intermediate heating to 300 °C for 10 min, as well as repeated cycles of only HCl exposure and repeated cycles of only 300 °C heating. The hydroxyl concentration increased upon repeated exposure to HCl gas without intermediate heating, demonstrating that HCl led to significant hydrolysis. Heating steps after the HCl exposure largely reversed the HCl-driven hydrolysis. The trends for the HCl-treated samples with and without intermediate heating approached each other after a final heating step to bring all samples on a total of 16 h at 300 °C. In both cases, part of the HCl-driven hydrolysis was preserved despite heating. This possibly indicates the existence of a non-zero optimal hydroxyl concentration for BTESE-derived materials. Incomplete condensation may be favorable for network relaxation.

Fig. 4c shows the shrinkage of BTESE-derived films after repeated cycles of exposure to HCl gas for 10 min with intermediate heating to 300 °C for 10 min, as well as repeated cycles of only HCl exposure and repeated cycles of only 300 °C heating. The shrinkage caused by constant heating at 300 °C is shown as reference. Repetitive heating to 300 °C led to somewhat more shrinkage as compared to constant heating. The increase was mainly visible after the first cycle, but the same cycling experiment executed with 30 min heating steps instead of 10 min (allowing more distinction) is shown in the inset of the graph and indicated repeatedly increased film shrinkage during alternate cooling and heating. Apparently, repetitive hydration and dehydration without a catalyst is already sufficient to induce network reorganization. This underlines the possibility of large-scale network evolution via back-and-forth bond breakage and reformation. Repetitive exposure to HCl gas without intermediate heating initially increased shrinkage, but the effect seemed to saturate after several cycles. The increase of film shrinkage by combining repeated HCl exposure with intermediate heating to 300 °C was more than the sum of the increased shrinkage of either step repeated separately. This synergetic effect of HCl exposure and heating corresponds with network optimization occurring in an iterative fashion, involving hydrolysis as well as condensation.

Fig. 4d shows the shrinkage of BTESE-derived films after four cycles of HCl exposure for 1 h and heating to 200 °C for 10 min, with varying periods of time in between heating and subsequent HCl exposure. Though the amount of moisture taken up by the organosilica material in this period was not controlled, the film with only 10 min rehydration time was expected to be less hydrated and indeed showed significantly less shrinkage than the film with > 45 min rehydration time. This observation corresponds with hydrolysis being the main contribution of HCl as observed with ^{29}Si DE-MAS-NMR. All in all, HCl treatments were found to significantly increase film shrinkage by catalyzing network hydrolysis. The treatments were most effective when applied in a repetitive fashion with intermediate heating and sufficient rehydration.

3.2. Chemical integrity

The integrity of the ethylene bridges throughout the HCl treatments was analyzed by ^{29}Si DE-MAS-NMR and FTIR. The relative intensity of the Q peak in the ^{29}Si DE-MAS-NMR spectra was 3–4% for all samples and did not increase, indicating no significant breakage of Si-C bonds during the post-treatments. The FTIR spectra confirmed the stability of the ethylene bridges by showing no changes in the 3000–2800 cm^{-1} C-H stretching vibrations [18], the 1459 cm^{-1} H-C-H scissoring vibrations [18] and the 1405 cm^{-1} and 1270 cm^{-1} C-H bending vibrations in Si-CH_2CH_2-Si [19–22]. Also, no HCl residues were observed. The ^{29}Si DE-MAS-NMR and FTIR spectra are shown in Figs. S1 and S2 in the

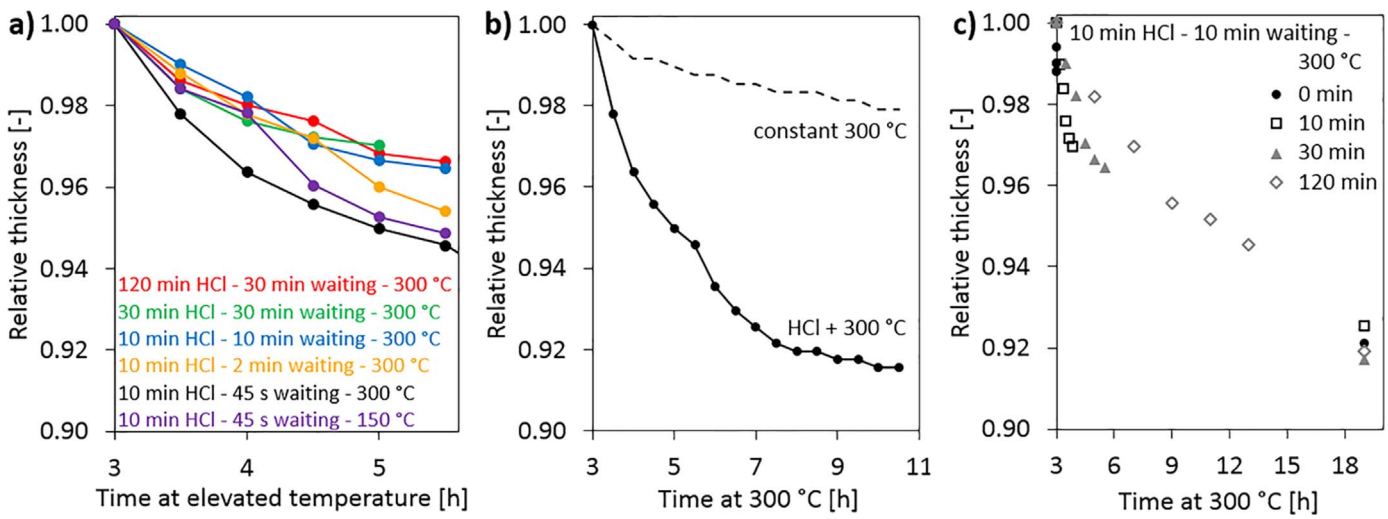

Fig. 5. Relative thickness of BTESE-derived films as measured with XRR at room temperature. Each data point represents one treatment cycle. a) Thickness monitored during five cycles of exposure to HCl gas for varying periods of time, waiting for varying periods of time, 30 min heating to 300 °C in N_2 or 150 °C in air and > 3 h rehydration in the ambient. b) Thickness monitored during 15 cycles of 10 min exposure to HCl gas, 45 s waiting, 30 min heating to 300 °C in N_2 and > 3 h rehydration in the ambient. The dotted line represents film shrinkage under constant heating. c) Thickness monitored during five cycles of 10 min exposure to HCl gas, 10 min waiting and heating to 300 °C in N_2 for varying periods of time.

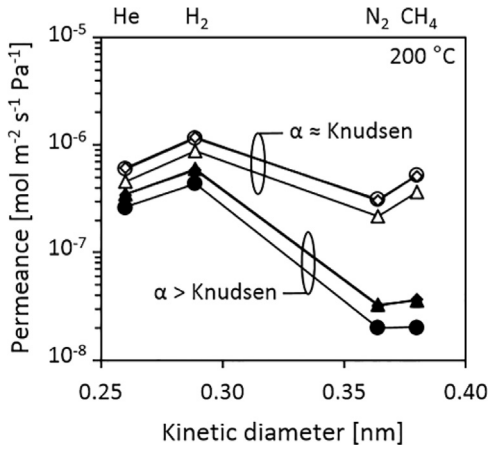

Fig. 6. Gas permeance versus kinetic diameter for BTESE-derived membranes with varying pore sizes, measured after consolidation at 300 °C in N_2 for 24 h and equilibration at 200 °C in the gas permeation set-up for 10 h. The symbols indicate which treatment the membranes received after data collection: no treatment (diamonds), 300 °C treatment (circles) or HCl and 300 °C treatment (triangles).

Supplementary material.

3.3. Effect of process variables

To investigate how the HCl-driven network evolution progresses in time, BTESE-derived films were repeatedly exposed to HCl gas for varying periods of time, kept in ambient atmosphere for varying periods of time and heated to 300 °C or 150 °C for 30 min. The results are shown in Fig. 5a and indicate a close to instantaneous effect of HCl with no benefit of exposure times longer than 10 min. This suggests deactivation of the catalyst or immobilization of the active species. Very short waiting periods between taking the sample out of the HCl atmosphere and heating it increased the shrinkage. Possibly, HCl residues were still present in the film and catalyzed reactions with increasing rates upon heating. This would also suggest that most HCl diffuses out of the film within minutes. Rapid heating to 150 °C yielded almost the same degree of shrinkage as rapid heating to 300 °C.

Fig. 5b shows the shrinkage of a film during 15 cycles of HCl exposure for 10 min and intermediate heating to 300 °C for 30 min. After about 10 cycles the shrinkage largely stopped. However, no complete stabilization of the structure was achieved; subsequent heating to 300 °C for 60 h still led to about 4% additional shrinkage.

The progress of condensation during the intermediate heating steps was investigated by repeatedly exposing films to HCl for 10 min with varying periods of heating to 300 °C in between. A final heat treatment was done to bring all samples at the same total period of time at 300 °C to enable fair comparison. Results are shown in Fig. 5c. Remarkably, the sample without intermediate heating (0 min) initially stayed behind in shrinkage but achieved the same effect as the other samples once it was heated at the end. This can be explained by accumulating HCl-driven hydrolysis that yields some initial shrinkage but then requires condensation to achieve the full potential of network reorganization. All in all, HCl-driven hydrolysis was found to be approximately instantaneous and accumulative, though reaching full network stabilization is a challenge.

3.4. Micropore structure

Single-gas permeation measurements were done on BTESE-derived membranes with He, H_2, N_2 and CH_4 as permeating gases to analyze the evolution of the micropore structure. Two sets of membranes were prepared with different pore sizes. All membranes were preheated in an oven at 300 °C in N_2 for 24 h. Gas permeation was measured at 200 °C under continuous steady-state conditions for 16 h. Fig. 6 shows the permeance versus kinetic diameter of the permeating gas molecules for both sets of membranes. One set showed H_2/N_2 and H_2/CH_4 selectivities of 17–22, comparable to values reported elsewhere [6,23] and well above the Knudsen values (theoretical values 3.6 for H_2/N_2 and 2.8 for H_2/CH_4). This indicates that the permeance of N_2 and CH_4 molecules was hindered by a size exclusion mechanism. Based on the kinetic diameters of the gas molecules (He 0.26 nm, H_2 0.29 nm, N_2 0.36 nm, CH_4 0.38 nm) [24] the effective pore size was estimated to be around 0.3 nm. The other set of membranes showed H_2/N_2 and H_2/CH_4 selectivities around the Knudsen values, indicating absence of size exclusion and an effective pore size larger than 0.4 nm.

Following the first 16 h of gas permeation, some membranes were taken out of the permeation set-up, subjected to either a HCl treatment and heating to 300 °C in N_2 for 60 h or only heating to 300 °C in N_2 for 60 h, and placed back in the permeation set-up for continuous steady-state permeation at 200 °C for a total of 78 h. The membranes were then taken out of the permeation set-up again for a second heating step at 300 °C for 60 h and the permeation was measured again at 200 °C for a

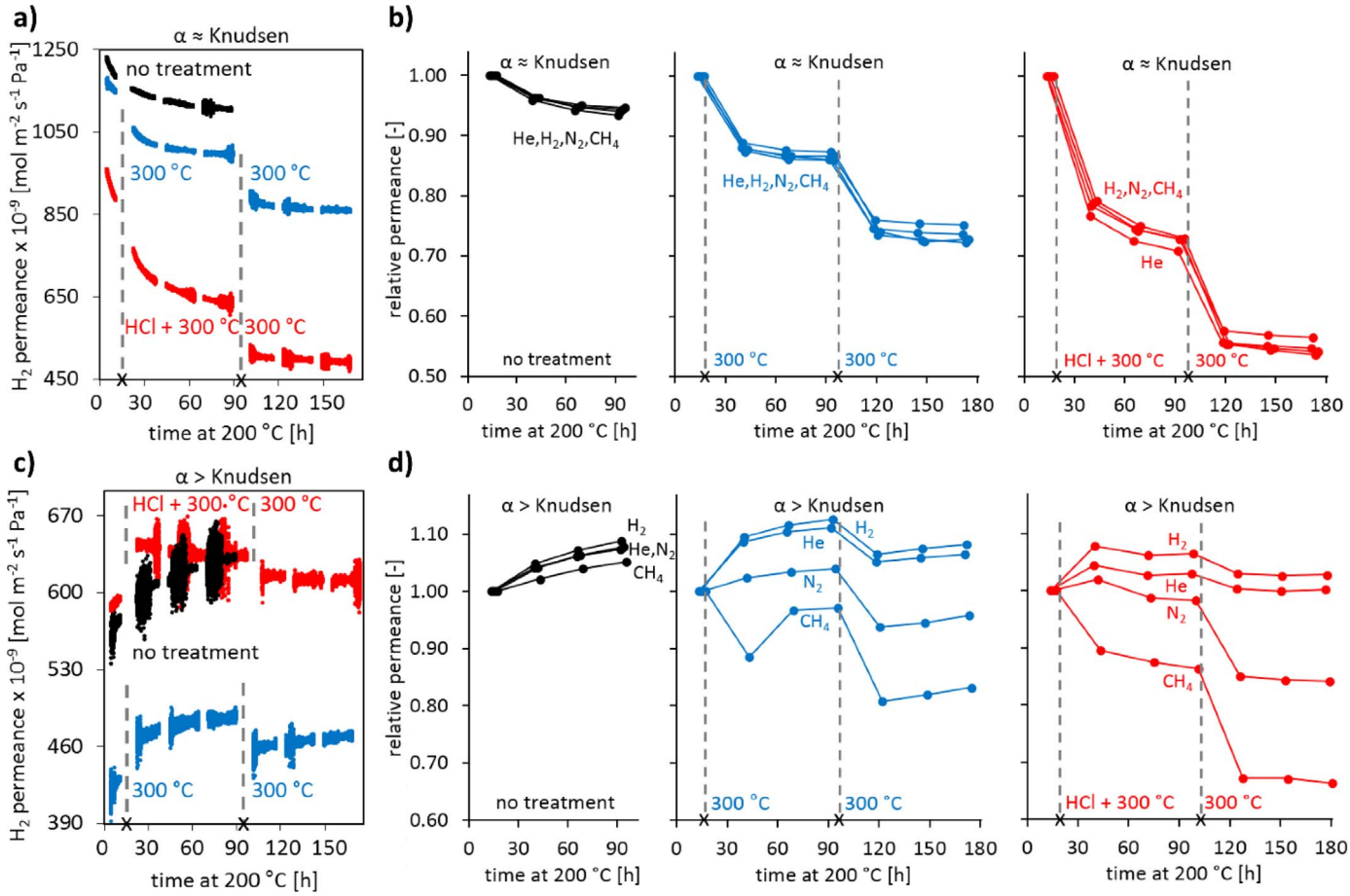

Fig. 7. In-situ GP data at 200 °C of BTESE-derived membranes with effective pore sizes of > 0.4 nm and ~0.3 nm after consolidation at 300 °C in N_2 for 24 h. After 16 h of continuous permeation, some membranes were temporarily taken out of the permeation set-up for a HCl treatment and heating to 300 °C for 60 h (red) or for only heating to 300 °C for 60 h (blue). The HCl treatment involved eight cycles of exposure to HCl for 30 min, immediate heating to 150 °C in air for 30 min and rehydration in a humidified atmosphere for at least 2 h. After another 78 h of continuous permeation, the membranes were heated again to 300 °C for 60 h. The treatments are indicated in the graphs by crosses on the x-axis and vertical dotted lines. a) Permeance of H_2 through membranes with effective pore sizes > 0.4 nm during consecutive continuous periods of 10–19 h. b) Relative permeance of He, H_2, N_2 and CH_4 through membranes with effective pore sizes > 0.4 nm. c) Permeance of H_2 through membranes with effective pore sizes ~0.3 nm during consecutive continuous periods of 10–19 h. d) Relative permeance of He, H_2, N_2 and CH_4 through membranes with effective pore sizes ~0.3 nm. (For interpretation of the references to color in this figure legend, the reader is referred to the web version of this article.)

total of 78 h. The HCl treatment involved eight cycles of exposure to HCl for 30 min, immediate heating to 150 °C in air for 30 min and rehydration in a humidified atmosphere for at least 2 h.

Fig. 7a shows the permeance of H_2 during 10–19 h intervals for the membranes with effective pore sizes > 0.4 nm. The permeance of the membrane without intermediate HCl treatment or heating to 300 °C decreased throughout the entire experiment time at 200 °C. This demonstrates the subtle but persistent structural instability of the material after synthesis and consolidation at 300 °C for 24 h. As discussed in our previous report [10], the ongoing decrease in permeance can be explained with a slowly increasing number of network linkages and a slow effective densification of the pore structure. This decay in permeance also confirms that there were no pinhole defects dominating the membrane performance, because pinholes are not expected to close under these conditions. The permeance of the membrane with additional intermediate heating to 300 °C showed an ongoing decrease that was enforced by both treatments. The even stronger permeance decay of the membrane with intermediate HCl treatment and heating to 300 °C showed the catalyzing effect of HCl on the pore evolution. It demonstrated the potential result of the subtle instability; a permeance reduction of about 45% occurred in the second and third stage of the experiment. Differences in absolute permeance values at the beginning of the experiments are within the range of common membrane-to-membrane variations. In the first hours at 200 °C (before additional treatments) the flux decay varied somewhat for the different membranes. This could be due to removal of varying extents of adsorbed water from the pores, but may also indicate that the membrane subjected to HCl treatment started with the largest instability and that the apparent influence of HCl was somewhat smaller in reality. Fig. 7b shows the relative permeance of He, H_2, N_2 and CH_4 after each 10–19 h H_2 interval, indicating that the changes in permeance were identical for all gases. The absolute permeance values are listed in Table S1 in the Supplementary material. No transition from Knudsen diffusion to size exclusion was observed, indicating that any densification around bottlenecks did not lead to significant formation of small size-selective pores ~0.3 nm.

Fig. 7c shows the permeance of H_2 during the 10–19 h intervals for all membranes with effective pore sizes ~0.3 nm. The permeance of the membrane without intermediate HCl treatment or heating to 300 °C increased throughout the entire experiment time at 200 °C, indicating that these smaller pores widened or opened. As discussed in our previous study [10], pores ~0.3 nm are so narrow that hydroxyl groups at the pore surface are likely to sterically hinder passing gas molecules. In this situation the net loss of bulky oxygen atoms due to ongoing condensation reactions (replacing two pendant hydroxyl groups by one bridging oxygen atom) can increase the permeance of inert gas molecules through those small pores. Therefore, despite the opposite trend in permeance as compared to larger pores > 0.4 nm, the observed

changes in pores ~0.3 nm can be explained within the same framework of ongoing condensation. A similar widening of pores ~0.3 nm has been observed by means of positron annihilation spectroscopy in purely inorganic silica (amorphous SiO_2) for increasing calcination temperatures [25]. The permeance of the membrane with additional intermediate heating to 300 °C showed an ongoing increase that was enforced by both heating steps. The permeance of the membrane with intermediate HCl treatment and heating to 300 °C demonstrated the catalyzing effect of HCl; the smaller pores rapidly widened or opened (removal of pendant hydroxyl groups) and then showed a transition towards a decreasing permeance due to overall pore structure densification. Such overall densification also occurred in the Knudsen-type membranes with effective pore sizes > 0.4 nm and affected the permeation channels on a longer time scale than pore widening.

Fig. 7d shows the relative permeance of He, H_2, N_2 and CH_4 through the membranes with effective pore sizes ~0.3 nm after each 10–19 h H_2 interval (see Table S1 in the Supplementary material for the absolute permeance values). Significant discrimination between larger and smaller molecules occurred. The larger pores appeared to be more sensitive to overall densification and larger molecules may benefit less from the widening or opening of the smallest pores. The increasing selectivity for smaller molecules corresponds with previous reports on vapor-phase HCl treatments of BTESE-derived membranes [11,12]. All in all, HCl treatments could accelerate both the widening or opening of the smallest pores and the densification of the overall pore structure, unveiling a remarkable potential for change in the material. Though ongoing changes in permeance of the membrane with HCl treatment are hardly visible after the second heating step, complete stabilization of the pore structure may not be achieved. Nevertheless, the acceleration of the pore evolution demonstrates the effectiveness of the approach of iterative hydrolysis and condensation. Optimization of this process for specific membrane devices enables improving the long-term performance stability.

The ongoing reorganization of the material structure raises the question to what end state the network is evolving. The Si-O-Si bond angles are known to be able to vary over 40° [26] and thus form significant amounts of non-optimal network linkages. These have the potential to take on energetically more favorable conformations when the required energy is supplied. The non-reversible nature of the observed network evolution indeed points towards relaxation and not only to a shift in the equilibrium between condensation and hydrolysis due to changing environments. The observations of a possible non-zero optimum in hydroxyl concentration (Fig. 4b) and of pores ~0.3 nm widening or opening while the overall pore structure densifies (Fig. 7) also correspond with network relaxation. Similar pore evolution has been reported for sol-gel-derived inorganic silica, with pores ~0.3 nm increasing in size and pores ~0.8 nm and ~1.2 nm decreasing in size upon heat treatment [25]. The ideal connectivity and pore size may be dictated by the spacing ethylene bridges. Molecular dynamics simulations of ethylene-bridged silica are reported to yield networks with a relatively broad pore size distribution with a maximum at approximately 0.25 nm, a shoulder at approximately 0.37 nm and reaching zero around 0.5–0.6 nm [27,28]. The ethylene bridges in these studies were randomly spread throughout the network and did not exactly mimic the experimental situation of each Si atom being bound to one ethylene bridge. The presence of the largest and smallest pores is thus probably overestimated. Nevertheless, the bimodal distribution does suggest the existence of preferential pore sizes and shows a local maximum in between ~0.3 nm and > 0.4 nm.

As for general applicability of the presented stabilization approach, in our previous study [10] the network evolution observed in ethylene-bridged silica was demonstrated to occur also in other organically bridged and inorganic silica structures. The approach of iterative hydrolysis and condensation is expected to facilitate network relaxation in any microporous (organo)silica material. As for the industrial applications of microporous organosilica membranes, these often involve liquid separation processes with retentate molecules of larger size than the gases used in the present study. This can cause identical membrane evolution to manifest differently in performance. Larger molecules will experience less additional hinder of ongoing pore shrinkage and the hinder for smaller molecules may become more important. This can result in a stable or even decreasing selectivity accompanying the flux decline instead of the increasing selectivity observed in the present study. Furthermore, industrial feed streams often contain water and depending on the operation conditions (temperature, acidity etc.) this will induce local rehydrolysis. This could then increase the steric hindrance of permeating species through the smallest pores, which could also be responsible for a slow (additional) flux decline. Such environment-dependent equilibration issues may be solved by periodical regenerative treatments.

4. Conclusion

Structural evolution of BTESE-derived networks is strongly accelerated by repeated exposure to HCl gas alternated with heating, which induces iterative hydrolysis and condensation. XRR indicated increased shrinkage in BTESE-derived films. ^{29}Si DE-MAS-NMR and FTIR of BTESE-derived powders indicated no degradation of the ethylene bridges and increasing hydroxyl concentrations upon exposure to HCl, demonstrating that HCl predominantly catalyzed hydrolysis of siloxane bonds. GP of BTESE-derived membranes indicated accelerated widening or opening of the smallest pores and densification of the overall pore structure. This yielded changes of as much as 45% in permeance. The networks were not fully stabilized after being at 200–300 °C for up to 12 days, but material evolution was pushed significantly further towards its end state. The approach of iterative hydrolysis and condensation is effective for network relaxation and enables improvement of the long-term performance stability of BTESE-derived molecular sieving membranes. Using gaseous HCl eliminates the risk of material dissolution and pinhole formation related to wet- or vapor-phase catalyst treatments.

Acknowledgements

Financial support from the Advanced Dutch Energy Materials (ADEM) program of the Dutch Ministry of Economic Affairs, Agriculture and Innovation is gratefully acknowledged. Support from the Dutch Organization of Scientific Research (NWO) for the solid-state NMR facility for advanced materials science in Nijmegen is gratefully acknowledged.

Appendix A. Supporting information

Supplementary data associated with this article can be found in the online version at http://dx.doi.org/10.1016/j.memsci.2017.11.014.

References

[1] H.L. Castricum, A. Sah, R. Kreiter, D.H.A. Blank, J.F. Vente, J.E. ten Elshof, Hydrothermally stable molecular separation membranes from organically linked silica, J. Mater. Chem. 18 (2008) 2150–2158.
[2] H.L. Castricum, R. Kreiter, H.M. van Veen, D.H.A. Blank, J.F. Vente, J.E. ten Elshof, High-performance hybrid pervaporation membranes with superior hydrothermal and acid stability, J. Membr. Sci. 324 (2008) 111–118.
[3] H.L. Castricum, A. Sah, R. Kreiter, D.H.A. Blank, J.F. Vente, J.E. ten Elshof, Hybrid ceramic nanosieves: stabilizing nanopores with organic links, Chem. Commun. (2008) 1103–1105.
[4] R. Kreiter, M.D.A. Rietkerk, H.L. Castricum, H.M. van Veen, J.E. ten Elshof, J.F. Vente, Stable hybrid silica nanosieve membranes for the dehydration of lower alcohols, ChemSusChem 2 (2009) 158–160.
[5] M. Kanezashi, K. Yada, T. Yoshioka, T. Tsuru, Design of silica networks for development of highly permeable hydrogen separation membranes with hydrothermal stability, J. Am. Chem. Soc. 131 (2009) 414–415.
[6] H.L. Castricum, G.G. Paradis, M.C. Mittelmeijer-Hazeleger, R. Kreiter, J.F. Vente, J.E. ten Elshof, Tailoring the separation behavior of hybrid organosilica membranes by adjusting the structure of the organic bridging group, Adv. Funct. Mater. 21

(2011) 2319–2329.
[7] M. Kanezashi, S. Miyauchi, H. Nagasawa, T. Yoshioka, T. Tsuru, Pore size control of Al-doping into bis (triethoxysilyl) methane (BTESM)-derived membranes for improved gas permeation properties, RSC Adv. 3 (2013) 12080–12083.
[8] R. Xu, M. Kanezashi, T. Yoshioka, T. Okuda, J. Ohshita, T. Tsuru, Tailoring the affinity of organosilica membranes by introducing polarizable ethenylene bridges and aqueous ozone modification, ACS Appl. Mater. Interfaces 5 (2013) 6147–6154.
[9] H.M. van Veen, M.D.A. Rietkerk, D.P. Shanahan, M.M.A. van Tuel, R. Kreiter, H.L. Castricum, J.E. ten Elshof, J.F. Vente, Pushing membrane stability boundaries with HybSi® pervaporation membranes, J. Membr. Sci. 380 (2011) 124–131.
[10] A.P. Dral, K. Tempelman, E.J. Kappert, L. Winnubst, N.E. Benes, J.E. ten Elshof, Long-term flexibility-based structural evolution and condensation in microporous organosilica membranes for gas separation, J. Mater. Chem. A 5 (2017) 1268–1281.
[11] J. Wang, G. Gong, M. Kanezashi, T. Yoshioka, K. Ito, T. Tsuru, Pore-size tuning of highly selective organic-inorganic hybrid silica membranes by solid-phase post-treatment at low temperature, Chem. Lett. 41 (2012) 1663–1665.
[12] J. Wang, G. Gong, M. Kanezashi, T. Yoshioka, K. Ito, T. Tsuru, Pervaporation performance and characterization of organosilica membranes with a tuned pore size by solid-phase HCl post-treatment, J. Membr. Sci. 441 (2013) 120–128.
[13] H.P. Lin, C.Y. Mou, S.B. Liu, Ammonia hydrothermal treatment on mesoporous silica structure synthesized from acidic route, Chem. Lett. 28 (1999) 1341–1342.
[14] I.V. Melnyk, Y.L. Zub, E. Véron, D. Massiot, T. Cacciaguerra, B. Alonso, Spray-dried mesoporous silica microspheres with adjustable textures and pore surfaces homogenously covered by accessible thiol functions, J. Mater. Chem. 18 (2008) 1368–1382.
[15] H.P. Lin, C.Y. Mou, S. Bin Liu, Formation of mesoporous silica nanotubes, Adv. Mater. 12 (2000) 103–106.
[16] G. Gong, H. Nagasawa, M. Kanezashi, T. Tsuru, Tailoring the separation behavior of polymer-supported organosilica layered-hybrid membranes via facile post-treatment using HCl and NH_3 vapors, ACS Appl. Mater. Interfaces 8 (2016) 11060–11069.
[17] R.J.R. Uhlhorn, M.H.B.J. Huis in't Veld, K. Keizer, A.J. Burggraaf, Synthesis of ceramic membranes: Part I Synthesis of non-supported and supported y-alumina membranes without defects, J. Mater. Sci. 27 (1992) 527–537.
[18] G. Socrates, Infrared Characteristic Group Frequencies: Tables and Charts, 2nd ed, Wiley, Chichester, 1994.
[19] Y. Kayaba, F. Nishiyama, Y. Seino, T. Kikkawa, Molecular bonding structure of alkylene-bridged organosilicate glass films, J. Phys. Chem. C 115 (2011) 12981–12989.
[20] F. Hoffmann, M. Güngerich, P.J. Klar, M. Fröba, Vibrational spectroscopy of periodic mesoporous organosilicas (PMOs) and their precursors: a closer look, J. Phys. Chem. C 111 (2007) 5648–5660.
[21] U. Díaz-Morales, G. Bellussi, A. Carati, R. Millini, W. O'Neil Parker Jr., C. Rizzo, Ethane-silica hybrid material with ordered hexagonal mesoporous structure, Microporous Mesoporous Mater. 87 (2006) 185–191.
[22] V. Rebbin, M. Jakubowski, S. Pötz, M. Fröba, Synthesis and characterisation of spherical periodic mesoporous organosilicas (sph-PMOs) with variable pore diameters, Microporous Mesoporous Mater. 72 (2004) 99–104.
[23] H.F. Qureshi, A. Nijmeijer, L. Winnubst, Influence of sol-gel process parameters on the micro-structure and performance of hybrid silica membranes, J. Membr. Sci. 446 (2013) 19–25.
[24] D.W. Breck, Zeolite Molecular Sieves: Structure, Chemistry and Use, John Wiley & Sons, Inc, New York, 1974, pp. 593–724.
[25] M.C. Duke, S.J. Pas, A.J. Hill, Y.S. Lin, J.C. Diniz da Costa, Exposing the molecular sieving architecture of amorphous silica using positron annihilation spectroscopy, Adv. Funct. Mater. 18 (2008) 3818–3826.
[26] D.S. Wragg, R.E. Morris, A.W. Burton, Pure silica zeolite-type frameworks: a structural analysis, Chem. Mater. 20 (2008) 1561–1570.
[27] K.-S. Chang, T. Yoshioka, M. Kanezashi, T. Tsuru, K.-L. Tung, Molecular simulation of micro-structures and gas diffusion behavior of organic-inorganic hybrid amorphous silica membranes, J. Membr. Sci. 381 (2011) 90–101.
[28] T. Shimoyama, T. Yoshioka, H. Nagasawa, M. Kanezashi, T. Tsuru, Molecular dynamics simulation study on characterization of bis(triethoxysilyl)ethane and bis (triethoxysilyl)ethylene derived silica-based membranes, Desalin. Water Treat. 51 (2013) 5248–5253.